DOI: 10.13009/EUCASS2022-7473

Aerodynamic Characterization of In-Air Capturing Vehicles Using CFD Simulations

Yakut Cansev Kucukosman[1*], Silvania Lopes[1], Sophia Buckingham[1], Philippe Planquart[1]
Sunayna Singh[2], Leonid Bussler[2], Sven Stappert[2], Martin Sippel[2]

[1]*von Karman Institute for Fluid Dynamics VKI, 72 Chaussée de Waterloo, Rhode-St-Genèse B-1640, Belgium,*
**yakut.cansev.kucukosman@vki.ac.be*
[2]*DLR Institut für Raumfahrtsysteme, Linzer Straße 1, 28359, Bremen, Germany,* sunayna.singh@dlr.de

Abstract

The interest in recovering and reusing the rocket stages has given prominence to many innovative reusable launch technologies. One of the return modes, 'In-Air Capturing (IAC)' involves winged rocket stages captured mid-air and towed back to the launch site using an aircraft. One of the essential phases of IAC consists in maintaining the launcher and the towing aircraft in a parallel formation so that the capturing device navigates autonomously towards the launcher. To determine the optimum capturing configuration, a CFD methodology is proposed for building up a high-fidelity aerodynamic database instead of using empirical models for this purpose. First, the CFD flow solver is validated, and the best numerical settings are determined, before applying this approach to the individual vehicles in view of characterizing their aerodynamic performance as input to flight dynamic simulations.

1. Introduction

The concept of sustainability of high performance and high-cost rocket stages has drawn attention to many innovative return modes with the aim of recovering and reusing them. The commonly used recovery methods can be categorized as Vertical Take-off Vertical Landing (VTVL) and Vertical Take-off Horizontal Landing (VTHL). The currently operational and successful pioneers such as SpaceX and Blue Origin operate VTVL based Reusable Launch Vehicles (RLV) which require significant fuel consumption during landing [1]. The VTHL method based on winged RLVs can only glide back when there is sufficient energy (descending from orbit) and the ones powered by turbofans requires additional propulsion system which adds to stage mass [1, 2]. To overcome the challenges, an innovative approach called 'In-Air-Capturing (IAC) was proposed and patented by DLR [3].

In IAC return mode where a reusable launcher vehicle (RLV) is towed back by an aircraft with the assistance of an Aerodynamically Controlled Capturing Device (ACCD) which helps to connect the two vehicles. This return mode is found to be more promising as it eliminates an additional propulsion system during the descent which reduces the mass and the cost of the system. Figure 1 shows a basic schematic of the complete operational cycle of IAC. After a vertical lift-off, the winged booster stage separates at Main Engine Cut-Off (MECO) and re-enters the atmosphere following a ballistic trajectory. At about 20 km altitude, it begins deceleration from supersonic velocity to a subsonic glide. Meanwhile, a towing aircraft loiters at 10 km altitude until the RLV reaches its vicinity. Between 8 km to 2 km, the IAC maneuver is performed [4]. The aircraft glides into a parallel formation with the RLV, such that the two vehicles have similar velocities and flightpath angles. During this formation flight, an ACCD attached by rope to the aircraft, autonomously captures the RLV. Then, the towing aircraft tows it back to the landing site [5]. In the vicinity of the runway, the stage is released to perform a horizontal landing.

DOI: 10.13009/EUCASS2022-7473

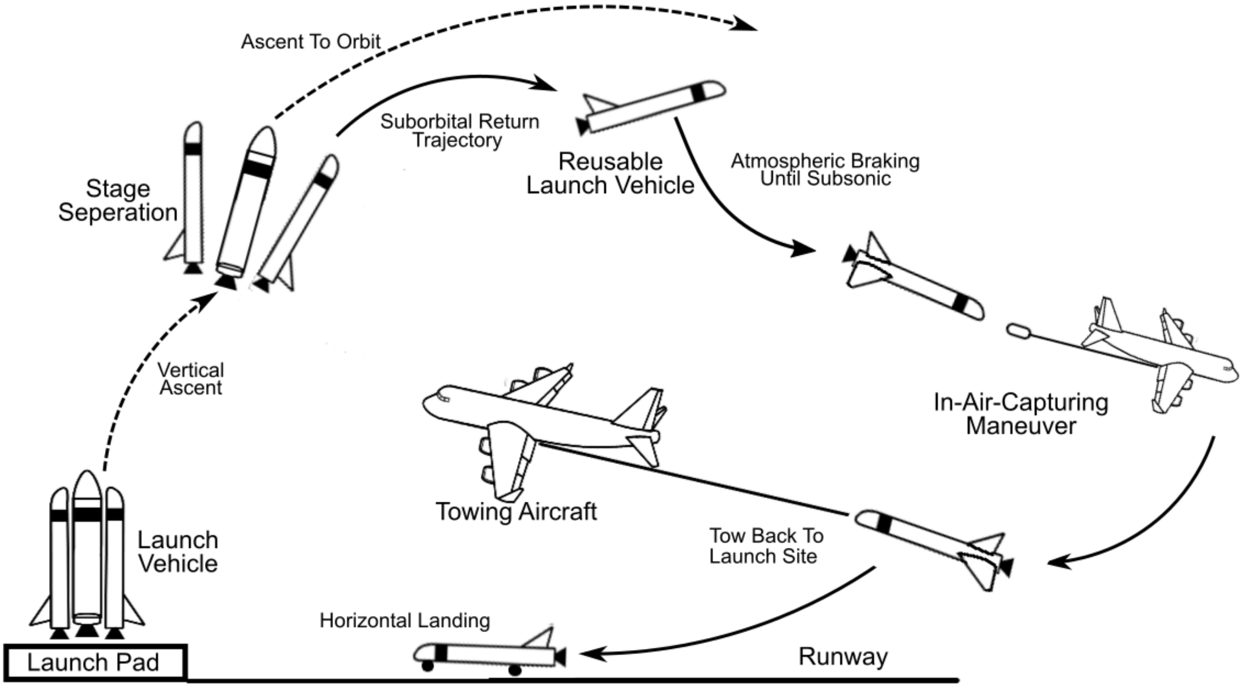

Figure 1:Complete IAC Cycle

The first and integral step of IAC requires the two vehicles to be in a parallel formation for at least 60s to enable the ACCD released from the aircraft to reach the RLV [1]. This would require both vehicles to maintain similar aerodynamic performance to achieve comparable velocities and altitude. Typical long-range commercial aircrafts have a lift to drag ratio between 17 to 19. However, during IAC, this ratio must be brought down to a value of around 6 for the vehicles to remain within the capture envelope. Empirical methods are used to determine the optimum capturing aircraft configurations by combining the drag generated by the various components [1]. However, the drag generating components as well as the vehicles wake create additional turbulence structures that the empirical methods are unable to estimate. Therefore, it is important to critically analyze the formation flight configurations using high-fidelity CFD simulations, while taking into consideration the atmospheric perturbations.

In this paper, the methodology for the high-fidelity simulations is presented. A sensitivity study is performed on the type of boundary conditions, the choice of the solver, the domain size and turbulence model, by referring to experimental results obtained on a NACA 0012 airfoil. Best practice guidelines are then applied to all three vehicles: the towing aircraft, the ACCD and the RLV alone, with the aim of providing reliable aerodynamic data for different angle of attacks. This paper is a part of H2020 FALCon project and continuation of the work by [1].

2. Validation of CFD methodology on NACA0012 profile

To establish a correct CFD methodology and to have confidence in the numerical solver and in its proper application, a validation study on the 2-D NACA0012 profile is performed and compared with the experimental results at the similar operating conditions (Mach no. 0.6, Reynolds no. 9×10^6). The sensitivity study is carried out on the domain size and the turbulence model which is then applied as a practical guideline to the three vehicles' simulations.

2.1. Domain size

Whenever compressible simulations are carried out, the acoustic field is also being solved. In order to avoid boundary conditions and acoustic wave reflections from the computational domain boundaries, a C-shaped type of domain has been used. In this respect, only two external boundaries are built: the inlet and the outlet. The inflow is represented by half of an ellipse and the outflow is simply a straight surface. Figure 2 shows a render of the selected computational domain.

Different domain size has been tested to assess whether the distance of the inflow and outflow boundaries might have an impact on the pressure field around the body. The results showed essentially no influence of the domain size on the pressure field for downstream length higher than 5 times the body domain (see Figure 3). This is expected due to the fact that if a domain without wall boundary conditions is used, blockage effect of side boundaries is avoided. In any case, just to ensure that the effect of domain size on turbulence development remains negligible, the boundaries were placed at a conservative distance of 5c and 10c in the upstream and downstream directions, respectively, where c is the length of the vehicle in question.

		x			
		5c	10c	20c	3c
y	5c	1	2	3	
	10c	4	5	6	
	20c	7	8	9	
	3c				10

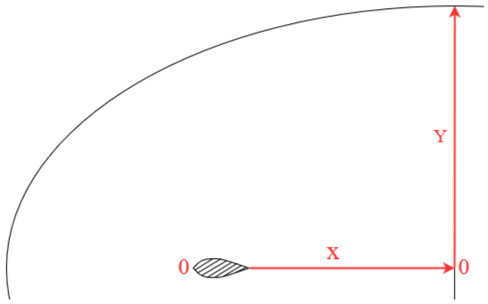

Figure 2: Coordinate combinations for domain size analysis.

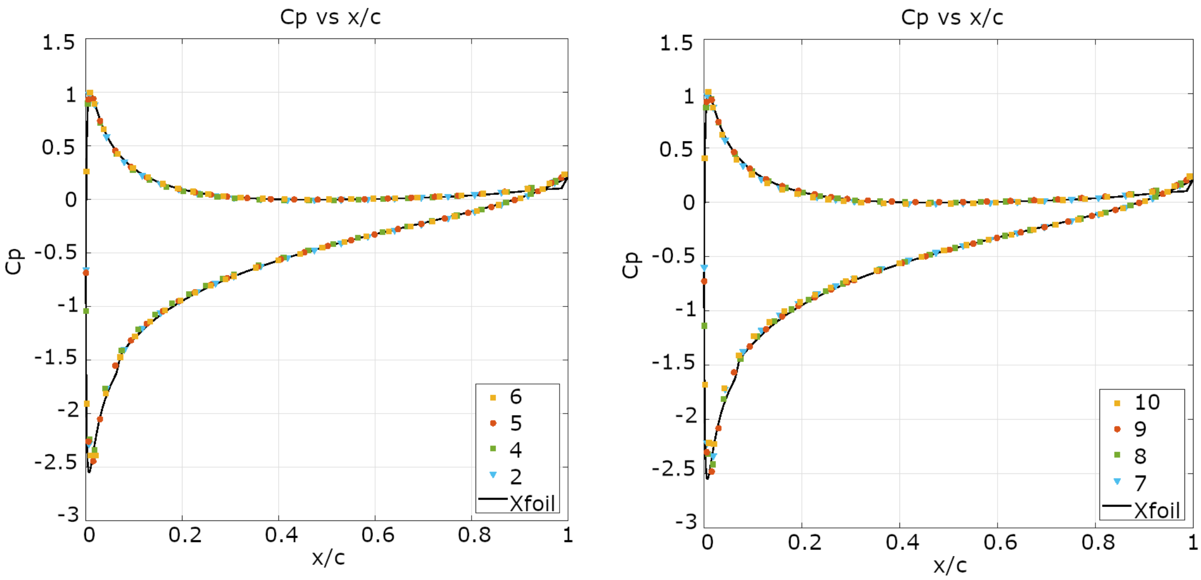

Figure 3: Pressure coefficient over airfoil- domain size analysis.

2.2. Turbulence model

Three different RANS models have been also tested, Spalart-Allmaras, k-epsilon and k-omega SST. The results have been compared against experimental data ([6]) and Xfoil outcomes. Detailed plot of the results is shown in Figure 4. As expected, the k-omega SST model provides the best fit when compared with experimental data and, therefore, it has been chosen for the CFD study on the vehicles.

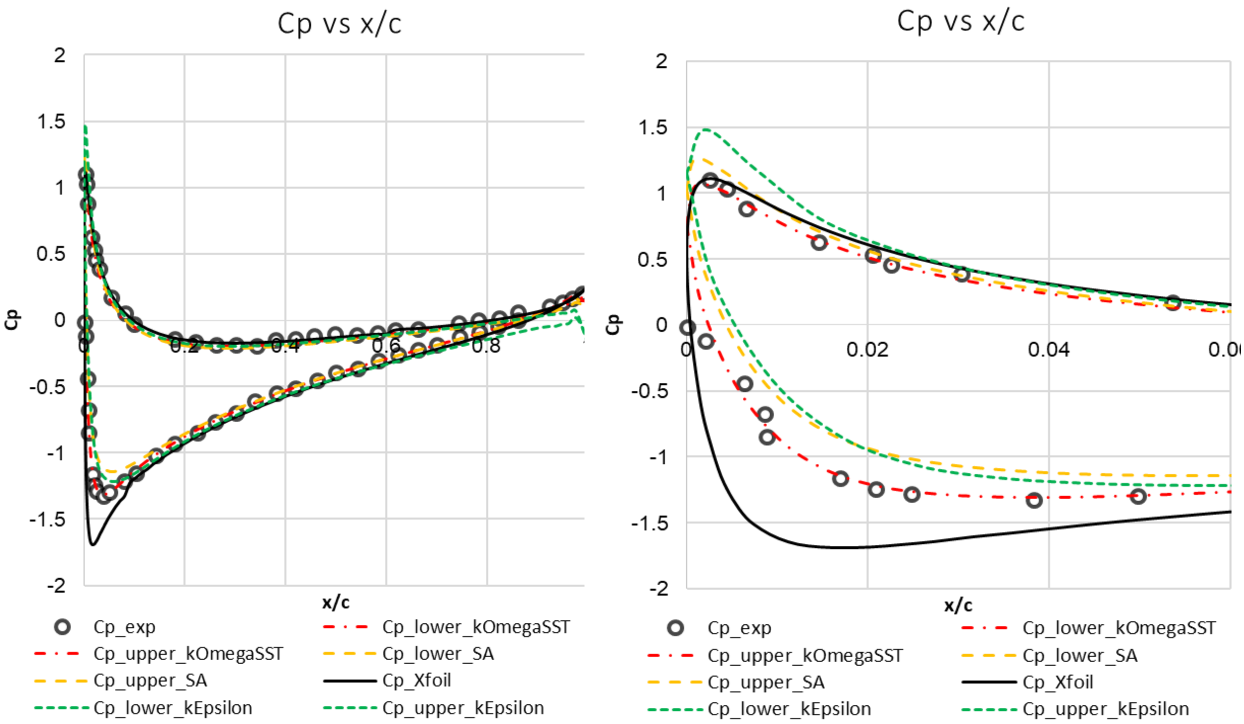

Figure 4: Pressure distribution over different turbulence models; along the chord (left) and zoomed to the leading-edge part (right).

3. CFD simulation for three vehicles: ACCD, towing aircraft, and RLV

The representation of the three vehicles after capturing the RLV is demonstrated in Figure 5 with the three vehicles: ACCD, towing aircraft and RLV.

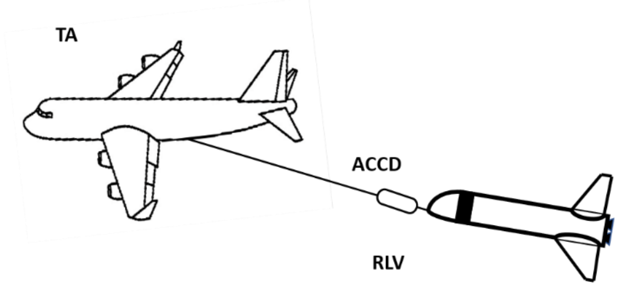

Figure 5: Representation of the three vehicles after capture.

- **Reusable Launch Vehicle (RLV):** Since typical commercial aircraft have a high Lift-To-Drag (L/D) ratio, the same should be maximised in RLV to allow successful formation. But a high L/D is usually achieved by increasing the wing span and size, which in turn decreases the payload capability. Therefore, a swept wing configuration was proposed to achieve a viable compromise between both requirements. The first stage for a 3 Stage-To-Orbit (3STO) launch vehicle (more details can be found in [7]) is selected. The stage mass during the descent is approximated to be about 80 tons.
- **Towing Aircraft (TA):** Based on the thrust requirements for towing a large RLV stage, a four engine, long range jetliner like the A340-600 was deemed fit [5].The retired aircraft comes with powerful Rolls Royce Trent 556 engines and large loading capacity to support the towing loads. It also has a relatively advanced flight control system that makes it suitable for IAC. However, in this paper, the engines are selected as CFM56.
- **Aerodynamically Controlled Capturing Device (ACCD):** This device is critical for the successful capture of RLV. For the current study, the ACCD is 2 m long with a cross-sectional diameter of 1.5 m. The four large fins, which can deflect up to a maximum of ±15° provide 6DOF agility and control. The nose of the ACCD is attached to the towing aircraft via rope and the back cone of the ACCD secures the connection with the RLV.

In this paper, the focus will be on the individual aerodynamic characterisation of the three vehicles rather than the investigating the interaction effects between them. This section provides the details about the CAD details, computational domain, and mesh sensitivity analysis for the three vehicles.

3.1. CAD of the three vehicles

The ACCD is a bluff body composed by a fuselage and 4 fins with symmetrical hexagonal profile (NACA0012 profiles), whose main dimensions are shown in Figure 6. The fins are equipped with flaps with 15% flap chord to fin chord ratio. The flaps are capable of independently deflecting from -15 to 15 degrees which allows the ACCD pitch yaw and roll controls.

Fins values		
Root chord length	[m]	1.434
Tip Chord length	[m]	0.9
Span	[m]	0.5
Leading edge sweep angle	[˚]	30.0
Flap Chod to fin Chord ratio	[%]	15

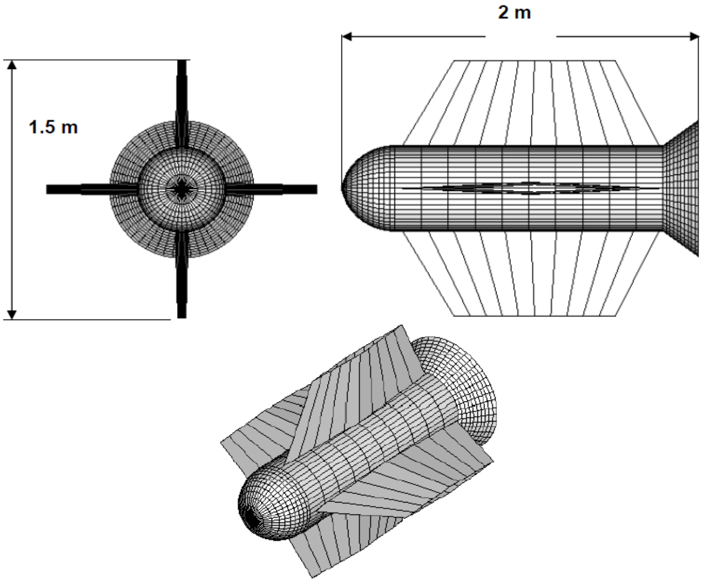

Figure 6: ACCD aerodynamic layout.

The cleaned CAD of the Airbus A340-600 which was used for the simulations is shown in Figure 7. Each component such as fuselage, wing, engine, landing gear, elevator, rudder and spoilers are provided in a separated '.stl' file to render the meshing process more flexible. Moreover, the trailing-edge of the wing, elevator and rudder is also defined in a separate '.stl' file to refine and better capture the sharp edges. The engine and landing gears have been simplified to facilitate the meshing procedure. This may also help in reducing numerical instabilities that can originate from poor quality meshed areas. In general, CAD cleaning has focused on removing unnecessary geometrical details that are considered to have a negligible influence on the flow features of interest.

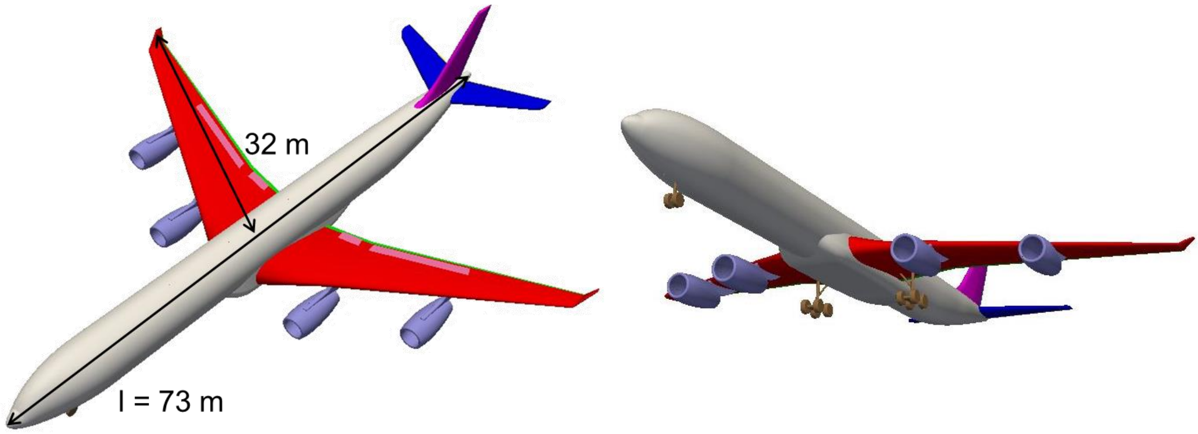

Figure 7: CAD of the Airbus A340-600.

DOI: 10.13009/EUCASS2022-7473

The same methodology described earlier for the Airbus A340-600 is applied. The CAD is divided in five different components such as fuselage, wing stab, wing tip, flap and booster and are provided in a separated 'stl' file for meshing (see Figure 8). Differently from the previous meshing strategy, the trailing-edge parts are not provided separately as the trailing-edges were rounded rather than sharp edges in the case of the Airbus.

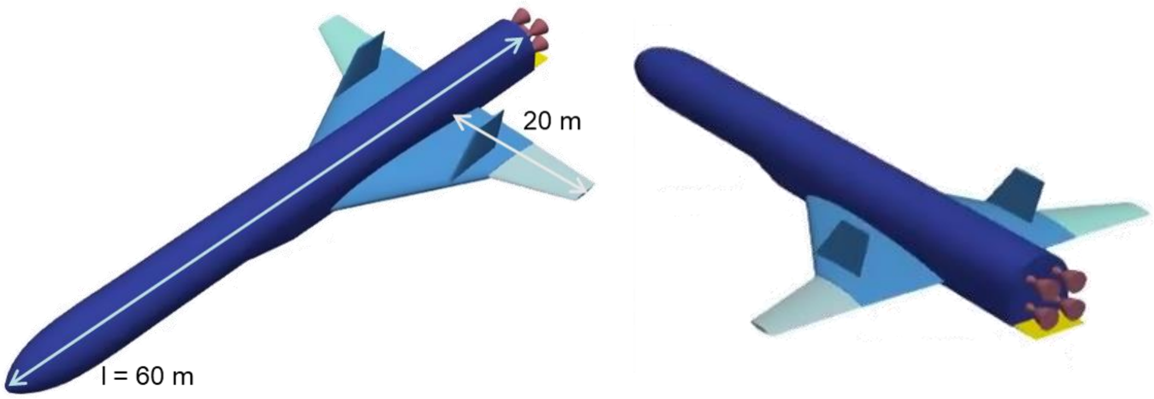

Figure 8: CAD of the RLV.

3.2. Computational domain and mesh generation

The computational domain consists of outer and inner domains. The outer domain, which embeds the inner domain, has a cone shape while the inner domain, where the vehicle is located, has a sphere shape (see Figure 9). By distinguishing these two different domains and having a cone-shaped inner domain, the angle of attack will be easily adjustable without having to re-mesh the domain, thus, reducing the computational efforts. In practice, the two subdomains are meshed separately, then the inner domain is rotated depending on the angle of attack and finally, the two are merged together. The same guidelines are applied for the domain size as explained in Section 2.1 and this methodology is applied to the three vehicles.

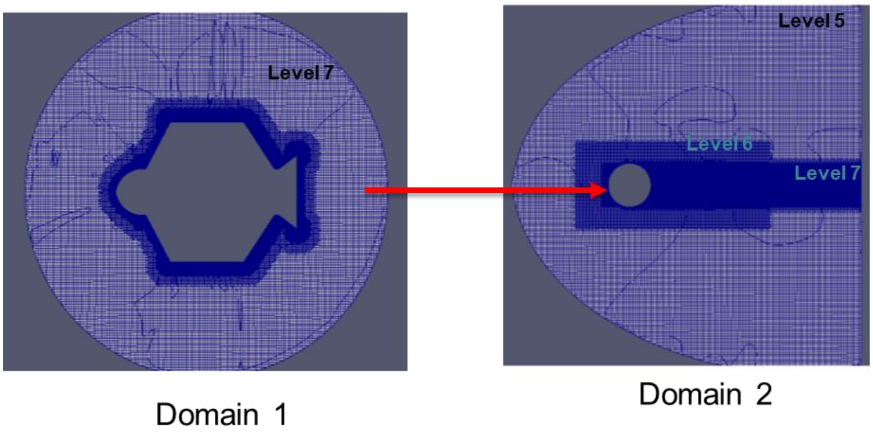

Figure 9: Computational domain: inner domain (left) and outer domain (right).

The mesh is created with snappyHexMesh, which is a mesh generation utility of OpenFOAM, consisting of predominant hexahedral (hex) and split-hexahedral (split-hex) cells with an option of boundary layer cells insertion on the surfaces. The mesh domains can be seen in Figure 9. It consists of three different refinement zones; the background mesh zone, the rectangle zone, which covers the wake and the sphere outer zone, and the inner sphere zone and the close wake. The gradual mesh refinement is applied to avoid discontinuity problems at the interfaces.

The mesh independence analysis is performed for three vehicles by changing the refinement levels of the sphere and wake zones, indicated in Figure 9. The Table 1 shows mesh sensitivity analysis for ACCD. The Grid-3 mesh size composed of 26 million cells is used for the CFD study. In order to use a wall function treatment to model the turbulent boundary layer, it is necessary to have the first cell height such that y^+ falls within the logarithmic layer, ~100 > y^+ > 30. In this case, the body wall mesh has an average y^+ of 78, thus ensuring that viscous wall effects are properly captured. The same mesh sensitivity analysis is performed for the towing aircraft and RLV.

Table 1: Mesh sizes used for mesh sensitivity analysis.

	Grid-1	Grid-2	Grid-3	Grid-4
# of cells	7M	15M	26M	37M
$V_{cell\_min}/V_{cell\_max}$	$6.62x10^{-9}/0.012$	$9.5x10^{-10}/0.012$	$9.54x10^{-10}/0.012$	$9.52x10^{-10}/0.012$
C_D	0.446(+4.2%)	0.432(+0.93%)	0.427(+0.2%)	0.428

3.3. Computational setup and boundary conditions

The air flows at M = 0.4 such that compressibility effects must be considered. The OpenFoam steady state three dimensional (3D) compressible RANS solver *rhoSimpleFoam* is used with second order discretization schemes to achieve higher accuracy in the results.

The boundary conditions applied to the domain are summarised in Table 2. In this study, the "inletOutlet" and "freeStream" boundary conditions have been used at the inlet. The inletOutlet boundary condition provides a generic outflow condition, with specified inflow for the case of return flow while the freeStream boundary condition provides a free-stream condition. It is a “mixed” condition derived from the inletOutlet condition, whereby the mode of operation switches between fixed (free stream) value and zero gradient based on the sign of the flux. On the interfaces between the two merged domains, a “cyclic AMI” boundary condition has been used. The turbulence intensity is fixed to T.I= 0.5% and the *k-omegaSST* turbulence model has been used.

Table 2: Boundary conditions.

	U [m/s]	p [Pa]	k [m2/s2]	ω [s-1]	T [K]
inlet	Freestream velocity	Freestream pressure	inletOutlet	inletOutlet	inletOutlet
outlet	Freestream velocity	Freestream pressure	inletOutlet	inletOutlet	inletOutlet
Body	No slip	$\nabla p=0$	Wall functions	Wall functions	$\nabla T=0$
interface	cyclicAMI	cyclicAMI	cyclicAMI	cyclicAMI	cyclicAMI
Freestream values	(0, 142.39,0)	47248.92141	0.7603	4.9584	249.15

3.4. Aerodynamic performance analysis for ACCD

The variation of lift and drag coefficients with angle of attack (AoA) are shown in Figure 10. The C_L curves have the generic form (essentially linear) with AoA over the whole range. The C_d curves show very small variation of C_d for small AoA. As the AoA increases, the C_d rapidly rises due to the increase of flow separation regions.

DOI: 10.13009/EUCASS2022-7473

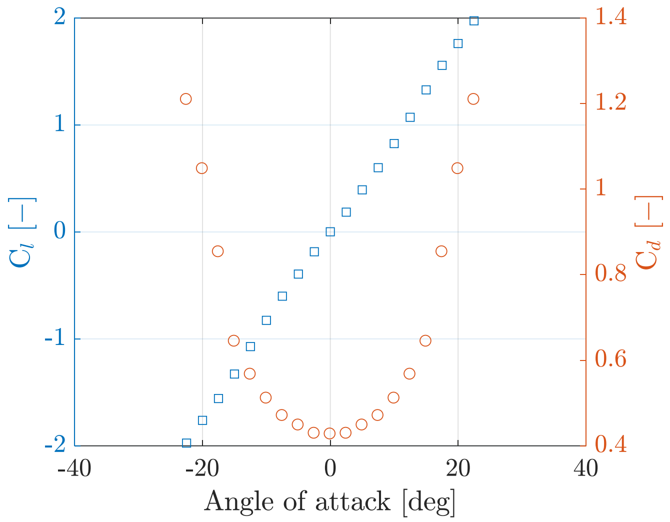

Figure 10: Lift and drag coefficients of ACCD.

A selection of flow field contours is presented here below, for 0 and -20 degrees angles of attack. Figure 11 shows the velocity magnitude fields in the symmetry plane of the longitudinal direction. It is possible to observe the stagnation point at the forehead of the body and the presence of a stagnating flow in the zone between the wing and the tail, due to blocking effect. Symmetric flow and a symmetric counter-rotating vortex is present for the AoA=0°, as can be seen by the streamlines in Figure 12. For AoA=20°, the flow and the vortex behind the body becomes completely asymmetric. The flow detachment from on the lower part of the wing is visualized by the streamline behaviour, indicating a possible loss of performance at this high angle of attack. An extensive characterisation of the aerodynamic performance of the ACCD is established by deflecting the fins horizontally (pitch), vertically (yaw) and opposite directions (roll) which can be found in [8].

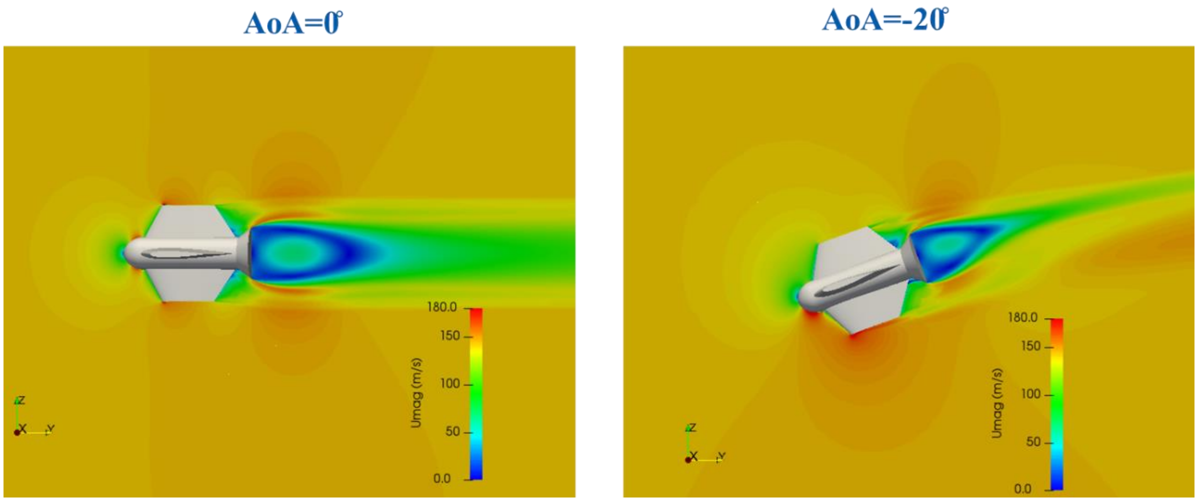

Figure 11: Velocity magnitude field contours at angles of attack 0° and -20°

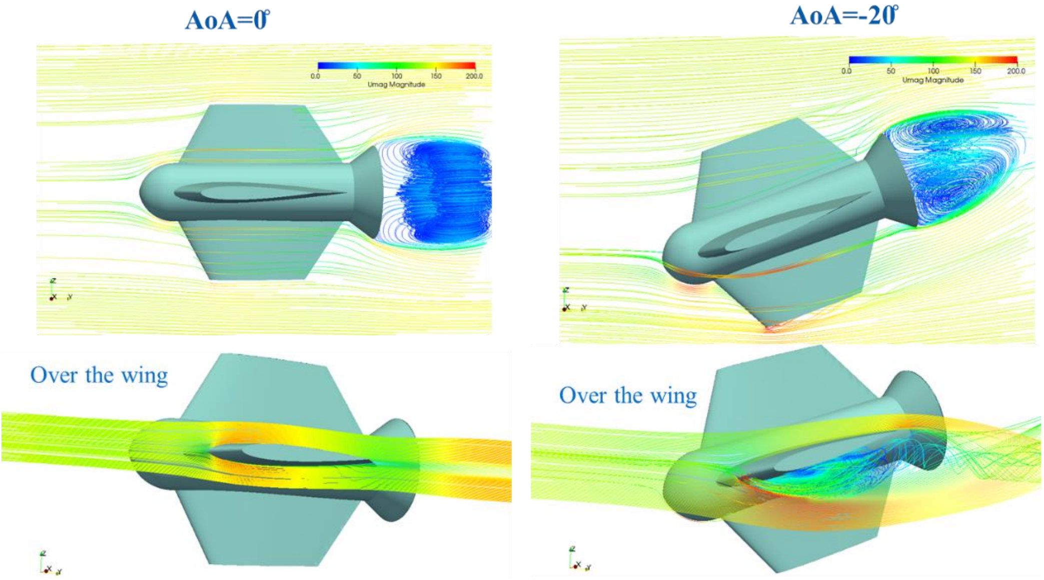

Figure 12: Streamlines at angles of attack 0° and -20°

3.5. Aerodynamic performance analysis for towing aircraft

The aerodynamic performance curve of the A340-600 obtained by CFD, covering a range of angles of attack from 0° to 10° with increments of 2°, is compared with the empirical predictions by DLR in Figure 13 where the coefficients of DLR are corrected with the reference area of VKI for results to be comparable. As expected, the lift and drag coefficients are increasing with increasing AoA. Although the trends obtained by VKI and DLR are similar, the values are higher in the predictions by DLR. The differences can be explained by the simplifications in the empirical modeling tool of DLR. Firstly, the tool does not consider the interaction between the components and secondly, the upper surface pressure is missing for the spoiler deflection. Thus, the analysis performed by VKI using CFD is necessary to obtain a more realistic performance curve by taking into account the aforementioned simplifications.

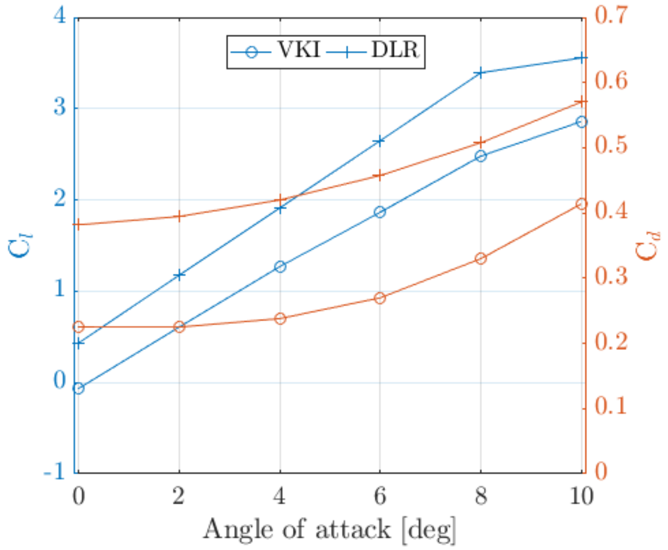

Figure 13: Lift and drag coefficients with respect to different angle of attacks in comparison with DLR predictions using empirical modelling.

When comparing the CFD predictions by VKI with the empirical results by DLR, one of the discrepancies observed is the negative lift coefficient at zero degrees angle of attack. To identify which surfaces are causing negative lift in the CFD, a deeper analysis is performed for the AoA=0° case by looking at the individual contributions from the different aircraft components, as tabulated in Table 3. The patches which contribute to the negative lift are found to be the fuselage, engines, gear and spoiler. It should be also noted that the different contributions cannot be compared as such,

DOI: 10.13009/EUCASS2022-7473

since here the total surface is used for calculating all of these coefficients, instead of their own surface area. From the pressure contour distribution along the bottom and top part of the aircraft, it is clear that the distribution of pressure is not symmetrical (see Figure 14). Higher pressure distributions are observed on the top view for the engines and the spoiler which therefore induce a negative lift on these surfaces. Although not as pronounced on the gear and fuselage, similar effects are observed with slightly higher pressure over the upper surfaces, thus resulting also in negative lift at AoA=0°.

Table 3: Drag and lift coefficients of the different aircraft components (*Reference area is kept as the total frontal area).

Patches	***Drag Coefficient****	***Lift Coefficient****
Fuselage	0.0295	-0.0199
Wing	0.0364	0.0917
Elevator	0.0062	0.0313
Rudder	0.0041	0.0023
Engines	0.0563	-0.0557
Gear	0.0398	-0.0002
Spoiler	0.0533	-0.1174

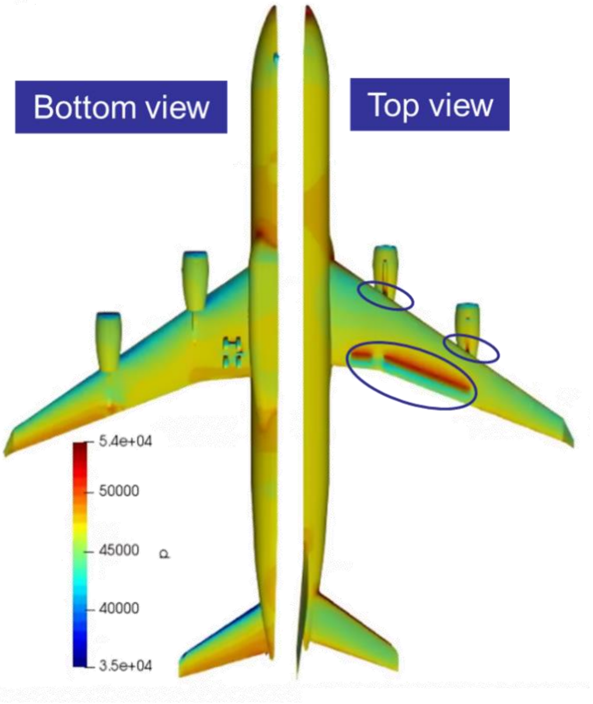

Figure 14: The pressure distribution along the Airbus.

The lift to drag ratio and the pitching moment in comparison with DLR's predictions are given in Figure 15 (left and right, respectively). In the calculation of the pitching moment, the reference length is chosen to be the length of the fuselage (L_{ref}=73 m) and the reference point is chosen to be the CoG of the Airbus (x, y, z = 0, 30.84, 0 m). The negative pitching moment states that the aircraft has an inherently stable behaviour. As stated earlier, the trends predicted by VKI using CFD agree with DLR's predicted trends. Some noticeable discrepancies observed on the pitch coefficients which can be attributed to the simplifications made by DLR's tool and the theoretical modelling approach. Nevertheless, the differences in the lift to drag ratio remain acceptable since these are less than 15% throughout the flight envelope.

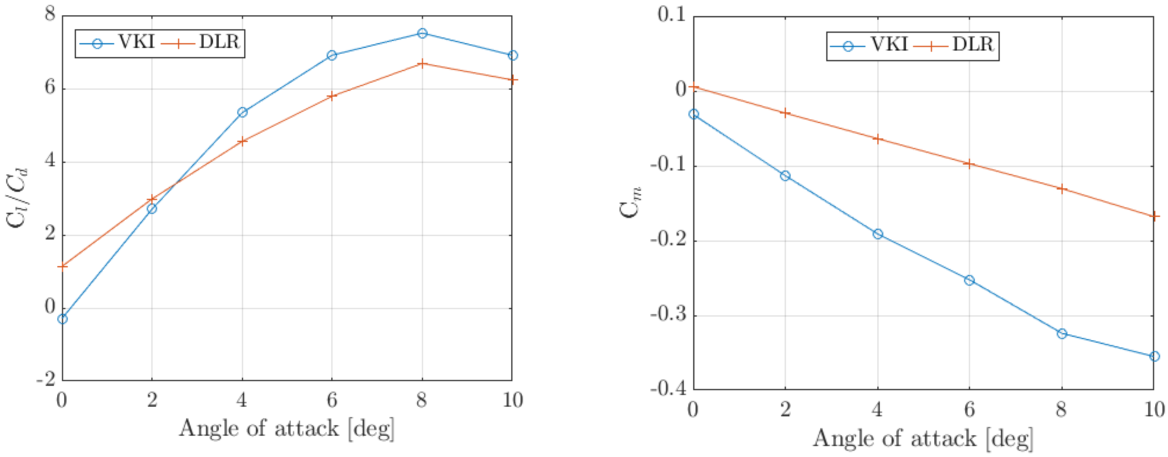

Figure 15: Lift to drag ratio (left) and the pitching moment (right) with respect to different angle of attack in comparison with DLR using empirical modelling.

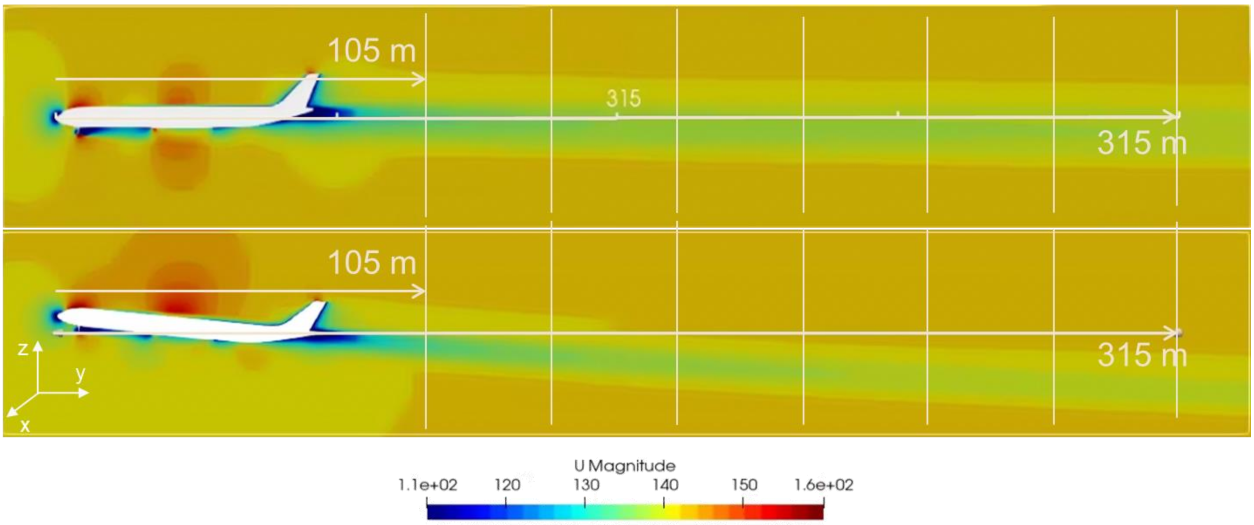

Figure 16: 2D contour plot of the towing aircraft in the symmetry plane for two different angles of attack; 0° (top) and 6 ° (bottom).

The 2D velocity contour plots of towing aircraft in the symmetry plane at 0° and 6° angles of attack is given in Figure 16. It has been observed that the wake deficit is still pronounced even further downstream (y/L > 4.5 where L is the length of the aircraft). Moreover, the width of the wake is highly influenced by the angle of attack. For further investigation, the streamwise and downwash velocity as well as the kinetic energy profiles of the two angles of attack are extracted at seven different streamwise locations (y/L= 1.5, 2.0, 2.5, 3.0, 3.5, 4.0 & 4.5) and showed in Figure 17. It can be observed that the streamwise velocity component is decaying faster than the downwash velocity component whereas downwash velocity component remains almost constant by reaching about 8% of free stream velocity at a distance of 315 m from the aircraft for an angle of attack of 6°. In addition, the downwash velocity component is influenced significantly by the angle of attack by increasing. The magnitude of the kinetic energy is found to be in the same order as the 0° AoA case while the higher AoA case is shifted downwards.

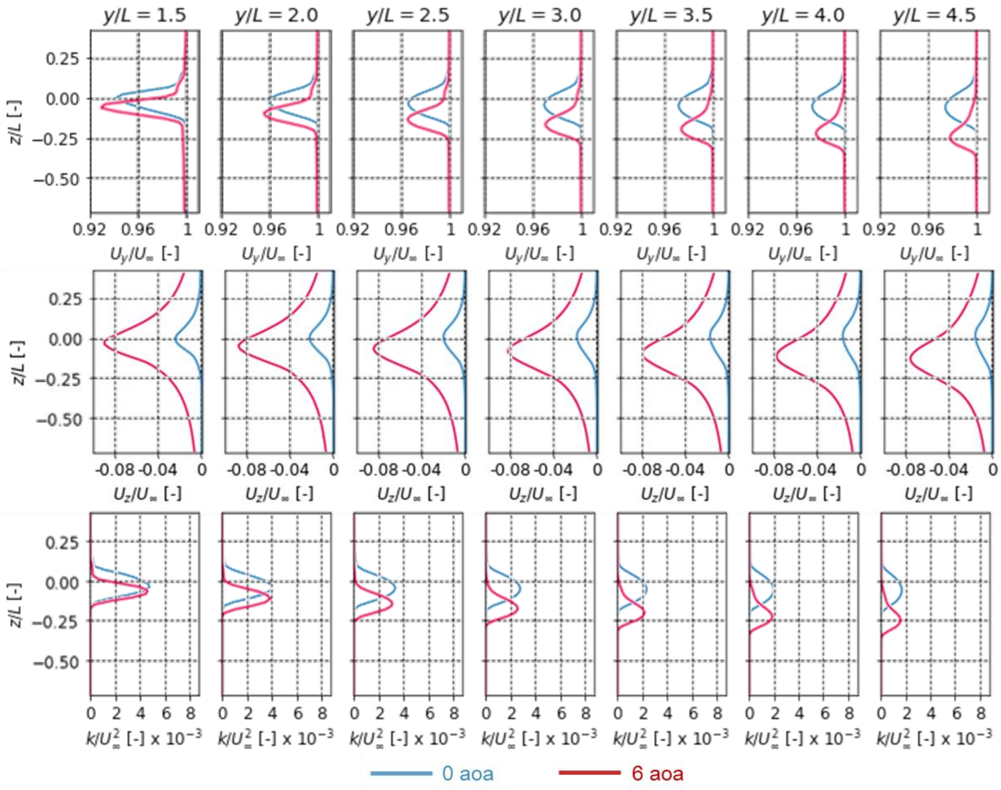

Figure 17: The wake profiles on the fuselage plane; streamwise velocity component (upper), the downwash velocity component (middle) and the turbulent kinetic energy (bottom) in comparison with 0° and 6° AoA

DOI: 10.13009/EUCASS2022-7473

3.6. Aerodynamic performance analysis for RLV

The aerodynamic performance curve and the pitching moment of the RLV with respect to different angles of attack are given in Figure 18. In the calculation of the pitching moment, the reference length is taken as the length of the fuselage (L_{ref}=60 m) and the reference point is chosen to be the CoG of the RLV (x, y, z = 0, 39.013, 0 m).

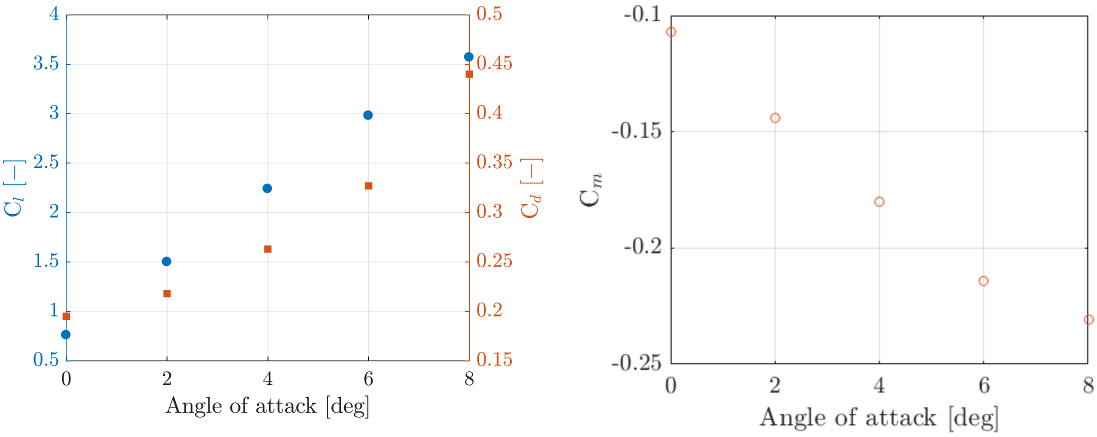

Figure 18: Lift and drag coefficients (left) and the pitching moment (right) of the RLV.

4. Conclusions

This paper describes the numerical guidelines to be applied for extracting reliable aerodynamic data by CFD simulations to be used as high-fidelity input for the dynamic modelling of the IAC application. For this purpose, the CFD methodology is validated by first simulating a 2D NACA0012 airfoil with the steady state RANS compressible solver *rhoSimpleFoam* in the CFD open-source code OpenFOAM and comparing the results to experimental data. The sensitivity analysis is performed by changing the domain size and the turbulence model. The effect of the domain size on the pressure field is found to be insignificant when the domain size is taken five times larger than the body length in the upstream direction. The turbulence model which provides the most accurate results is found to be the *k-omegaSST* model. Additionally, a meshing methodology is also established to reduce the computational effort by dividing the computational domain in two parts which enables to rotate the vehicle in a certain angle of attack without remeshing the whole domain. The mesh is generated using the OpenFOAM mesher *snappyHexMesh*, insertion boundary layer cells in the near wall region such that the first cell is found within the logarithmic region to properly capture the viscous wall effects. After the validation of the CFD methodology and meshing, 3D simulations are performed for the towing aircraft, the ACCD, and the RLV covering the operating range of incidences to obtain the aerodynamic curves. In the case of the towing aircraft, results are compared with the empirical tool, CAC. The trend of the curves is found to be similar but large differences in magnitude are observed. A more detailed analysis of the surface pressures over the different aircraft components was carried out, which highlighted interaction effects that are indeed neglected by the empirical model of DLR. Moreover, the pressure on the upper surface of the spoilers is not taken into account by the simplified approach, while by CFD these surfaces are found to produce negative lift due to an over-pressure. Furthermore, an extensive study is performed for higher angles of attack by refining the towing aircraft geometry in terms of wing, horizontal stabilizer and engine geometry.

Acknowledgements

This work was performed within the project '**F**ormation flight for in-**A**ir **L**auncher 1st stage **C**apturing demonstrati**on**' (**FALCon**) addressing development and testing of the "in-air-capturing" technology. FALCon, coordinated by DLR-SART, is supported by the EU within the Horizon2020 Programme 5.iii. Leadership in Enabling and Industrial Technologies – Space with EC grant 821953. Further information on FALCon can be found at http://www.FALCon-iac.eu

References

DOI: 10.13009/EUCASS2022-7473

[1] S. Singh, S. Stappert, L. Bussler, M. Sippel, S. Buckingham and C. Kucukosman, "A Full-Scale Simuation and Analysis of Formation Flight during In-Air-Capturing," in *72nd International Astronautical Congress*, Dubai, 2021.

[2] S. Sunayna, S. Madalin, S. Stappert, M. Sippe, S. Buckingham, S. Lopez and C. Kucukosman, "Control Design and Analysis of a Capturing Device Performing In-Air Capturing of a Reusable Launch Vehicle," in *9th European Conference for Aeronautics and Space Sciences (EUCASS)*, 2022.

[3] S. Stappert, J. Wilken, L. Bussler and M. Sippel, "A Systematic Assessment and Comparison of Reusable First Stage Return Options," in *70th International Astronautical Congress*, 2019.

[4] M. Sippel and J. Klevanski, "“Progresses in simulating the advanced in-air-capturing method," in *5th International Conference on Launcher Technology, Missions, Control and Avionics*, 2003.

[5] M. Sippel, S. Stappert, L. Bussler, S. Krause, S. Cain, J. Espuch, S. Buckingham and a. V. Penev, "Highly efficient RLV-return mode “In-Air-Capturing” progressing by preparation of subscale flight tests," in *n 8th European Conference For Aeronautics And Space Sciences (EUCASS)*, 2019.

[6] C. D. Harris, "Two-dimensional aerodynamic characteristics of the NACA 0012 airfoil in the Langley 8 foot transonic pressure tunnel," NASA Technical memorandum n 81927, 1981.

[7] S. Stappert, J. Wilken, L. Bussler and M. Sippel, "A systematic comparison of reusable first stage return options," in *8th European Conference For Aeronautics And Space Sciences (EUCASS)*, 2019.

[8] S. Singh, S. Stappert, S. Buckingham, S. Lopes, Y. Kucukosman, M. Simioana, M. Pripasu, A. Wiegand, M. Sippel and P. Planquart, "Dynamic Modelling and Control of an Aerodynamically Controlled Capturing Device for 'In-Air-Capturing'," in *11th International ESA Conference on Guidance, Navigation & Control Systems*, 2021.